First-principles thermal equation of state of fcc iridium

Kai Luo [*] and Ruifeng Lu

Institute of Ultrafast Optical Physics, Department of Applied Physics, Nanjing University of Science and Technology, Nanjing 210094, China

R. E. Cohen

Extreme Materials Initiative, Earth and Planets Laboratory, Carnegie Institution for Science, 5241 Broad Branch Road NW, Washington, DC 20015, USA

The thermal equation of states for fcc iridium (Ir) is obtained from first-principles molecular dynamics up to 3000 K and 540 GPa. The equation of state (EoS) is globally fitted to a simplified free-energy model and various parameters are derived. The theoretical principal Hugoniot is compared with shock wave experiments, where discrepancy suggests formation of new Ir phases. A few representative EoS parameters, such as bulk modulus K_T, thermal expansivity α, Grüneisen parameter γ, constant pressure capacity C_P, and Debye temperature Θ_D, are computed to compare with experimental data.

I. INTRODUCTION

Iridium (Ir) is a 5*d* transition metal of the platinum group. It is the second-densest metal with a density of 22.56 g/cm^3 at ambient condition, only slightly lower by about 0.12% than the densest metal osmium (Os). It has the largest shear modulus, $G = 210$ GPa, among the face-centered cubic (fcc) metals. The solid Ir remains in the fcc structure up to the melting point of 2719 K [1]. Due to its prominent thermophysical and mechanical properties and high corrosion resistance, it is used in many technological applications, such as crucibles, thermocouples, spark plugs, aircraft engine parts, and deep water pipes. The lack of phase transitions, simple fcc structure, high melting temperature, and nonreactivity make it ideal for experiments as a heater, absorber, or standard for example in diamond-anvil cell (DAC) experiments, and ideal for studying effects of compression on noble metals. Our understanding of the properties of Ir is still limited, and fundamental research on it remains of great interest.

With the advances in laboratory technologies, extreme conditions ($P > 200$ GPa, $T > 2000$ K) become more and more amenable to study. Fundamental to all studies at extreme conditions is the equation of state (EoS) that relates P, V, T, and U or F, where the symbols of P, V, T, U, and F stand for pressure, volume, temperature, internal energy, and Helmholtz free energy. The earliest investigation of iridium EoS dates back to 1937 by Bridgman up to 7 GPa [2,3], followed by work of Schock and Johnson [4] and then of Akella [5] up to 30 GPa. Cerenius and Dubrovinsky [6] measured the compressibility of Ir using DAC up to 65 GPa. Later, Cynn *et al.* found that Ir has the second-lowest compressibility of any

element after Os from their DAC experiment up to 65 GPa, which was corroborated by first-principles calculations [7].

For the EoS diagrams, zero-temperature first-principles EoS can be supplemented with finite-temperature vibrational entropies from the phonon dispersions. Phonon frequencies can be calculated from finite differences, or with the density functional perturbation theory (DFPT) [8]. Thanks to the development in the density functional theory toolkit, theoretical EoS for Ir appeared in several experimental works [7,9–12]. However, these theoretical EoS's were limited to low temperatures (around 300 K) using static calculations fitted to the Birch-Murnaghan (BM) EoS [13]. Anharmonic lattice vibrations were considered in Ref. [9], but the focus was the phase diagram and phase stability. Anzellini *et al.* studied Ir up to 80 GPa and 3100 K combining *in situ* synchrotron x-ray diffraction using laser-heating DACs and density functional theory calculations [14]. A comprehensive study covering a larger range of temperatures and pressures has not been performed. Indeed, studying other phases would be interesting, but in applications as a standard in experiments, we focus on the fcc phase. In this work, we aim to provide the EoS for fcc Ir up to 3000 K and 540 GPa in first-principles molecular dynamics (FPMD).

II. THEORETICAL EoS FROM FPMD

First-principles methods have been widely adopted in the simulation of condensed phases where no phenomenological parameters are needed. They give access to a space of thermodynamic conditions, which are hard to reach for experimental efforts and can be used to help calibrate experiments, where, for example temperature data are not sometimes available at the desired conditions. FPMD takes into account anharmonic vibrations of ions directly at finite temperatures through thermostatting. The electronic free energy is given
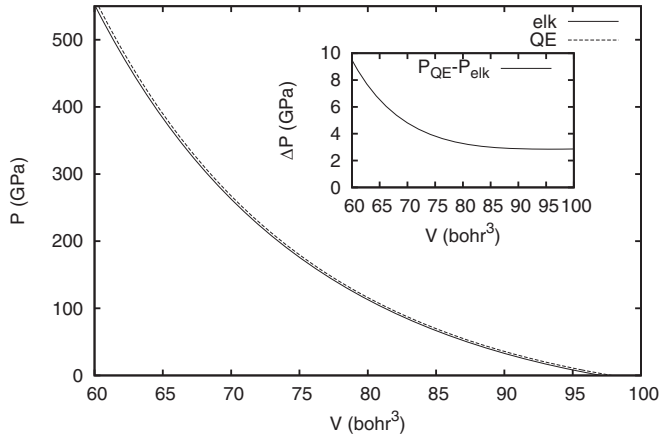
*kluo@njust.edu.cn

FIG. 1. Static equations of state from GBRV pseudopotential plane waves (QE) and LAPW (elk) calculation are compared. The Vinet EoS was used to fit the energy-volume curve. Inset figure shows the pressure difference and the maximum is less than 10 GPa.

by the Mermin-Kohn-Sham density functional theory (DFT) [15,16]. FPMD becomes the most used tool for predicting the thermal EoS, subject to the exchange-correlation free-energy functional approximations [17–19]. Classical molecular dynamics is suitable for high temperatures above the Debye temperature as it includes anharmonicity exactly, unlike other approaches. At lower temperature deviations from the P-V-T equation of state are small, but heat capacities and high-order properties such as thermal expansivity which show strong quantum effects at temperature below the Debye temperature are indeed less accurate.

A. FPMD details

First, we computed the static EoS of Ir at zero temperature. We used Quantum Espresso (ver. 6.7) throughout this work [20]. We used the scalar-relativistic Garrity-Bennett-Rabe-Vanderbilt (GBRV) ultrasoft pseudopotential [21] with the Perdew-Burke-Ernzerhof (PBE) exchange-correlation (xc) functional [22,23]. The electronic configuration for the pseudopotential is $[Xe]5p^{6.0}5d^{8.5}$. EoS was derived by fitting the energy-volume curve in the 3rd-order BM equation. To validate the range of applicability of the pseudopotential, we performed similar calculations in the linearized augmented plane wave (LAPW) code Elk [24] and the above two P-V curves agree well up to 550 GPa (see Fig. 1).

For the FPMD calculation, we prepared a cubic box containing 108 atoms in the fcc structure. The energy cutoffs for plane waves and density are 80 Ry and 320 Ry, respectively. Energy is converged within 5 meV per atom. Only the Γ point was sampled. The bands are occupied according to the Fermi-Dirac distribution at each temperature, and the number of bands is large enough to guarantee the occupation number is smaller than 10^{-7} for the highest occupied state. Early studies showed that the spin-orbit coupling does not affect the EoS and hence we used spin-unpolarized DFT neglecting spin-orbit coupling. Then conditions at a combination of lattice constants $a/a_0 = 0.86, 0.88, 0.90, 0.92, 0.96, 1.00$ ($a_0 = 3.801$ Å) and

temperatures $T = 300, 1000, 1500, 2000, 2500, 3000$ K were used in the simulations (see conditions in Table I). The time step is 20 a.u. (0.9676 fs). The equilibrated time steps are more than 2000 to get the statistical means and standard deviations, which give less than 1% standard deviation. The ionic temperature is regulated by the stochastic-velocity rescaling thermostat [25] and no quantum corrections to the ionic motion are included.

B. Free-energy model

We fit the Helmholtz free energy (F) as a function of V and T, $F(V, T)$. In FPMD, we have direct access to the variables of volume (V), temperature (T), pressure (P), and internal energy (U). Cohen and Gülseren [26] studied the thermal EoS of tantalum (Ta) in full-potential LAPW and mixed-basis pseudopotential methods. An accurate high-temperature global EoS was formed from the $T = 0$ K Vinet isotherm and the thermal free energy was fitted by the polynomial expansion in V and T (see Eq. (11) in Ref. [26]). De Koker and Stixrude [27] computed the free energy of MgO periclase and $MgSiO_3$ perovskite using FPMD, where the excess free energy was fitted in a similar expansion. Incorporating the Debye model [28], the total free energy is approximated by the polynomial expansion up to order N_i, N_j,

$$F(V, T) = \sum_{i,j=0}^{N_i, N_j} A_{ij} T^i (V^{-\frac{2}{3}})^j + F_0. \quad (1)$$

Neglecting the zero-point motion, $F_0 = k_B T[-D_3(x) + 3\ln(1 - e^{-x})]$, where a dimensionless parameter $x = \frac{\Theta_D}{T}$ with Debye temperature Θ_D. k_B is the Boltzmann constant. $D_3(x)$ is the third-order Debye function (see Appendix B). A_{ij} are fitting coefficients yet to be determined. For comparison, we mention the classical model, where $F_0 = -3k_B T \ln T$, with $T \ln T$ giving the proper classical behavior at low temperatures. That is, $C_V = 3k_B$ and $S = -\infty$ at 0 K. The Debye temperature Θ_D cannot be determined from the $U(T, V)$, $P(T, V)$ data from the classical molecular dynamics, so we obtain Θ_D from the root-mean-squared (RMS) displacements (see below). For simplicity, the Debye temperature at $P = 0$ GPa, $T = 300$ K is used.

III. RESULTS

We obtained the equilibrated quantities from FPMD, where U, P includes the ionic kinetic energy and ideal gas pressure, respectively. We subtracted each internal energy by the global minimum, as only the energy difference matters. The pressure and internal energy are $P = -(\frac{\partial F}{\partial V})_T$, $U = F + TS = F - T(\frac{\partial F}{\partial T})_V$. (U, P) data are grouped as a pair and fitted together to avoid bias between these two quantities. The fitting was performed using the weighted least-squares fit with the lm function including offset in the R language. Internal energy U and pressure P were fitted simultaneously to $F(V, T)$. $w = 1/\Delta^2$ is set for the weight, where Δ is the standard deviation of U and P. We fitted Eq. (1) with $N_i = 2$, $N_j = 3$. We analyzed the MD trajectories using the code VMD, and computed the RMSD for each run. From this we can obtain

TABLE I. Pressure P and internal energy per atom U and their standard deviations of the means P_{err} and U_{err} are extracted from FPMD simulations of fcc Ir for a given temperature T and atomic volume V (or the mass density ρ). The global minimum of U is underlined.

T (K)	V (bohr^3)	ρ (g/cm^3)	P (GPa)	P_{err} (GPa)	U (Ry)	U_{err} (Ry)
300	61.01	35.31	527.6	0.01	−181.353	0.00004
300	63.14	34.12	451.6	0.01	−181.423	0.00004
300	67.54	31.89	326.1	0.02	−181.538	0.00005
300	72.14	29.86	229.5	0.01	−181.624	0.00004
300	81.97	26.28	99.3	0.02	−181.729	0.00005
300	92.65	23.25	25.0	0.03	−181.770	0.00006
1000	61.01	35.31	531.3	0.04	−181.339	0.00012
1000	63.14	34.12	455.3	0.06	−181.410	0.00021
1000	67.54	31.89	330.0	0.04	−181.524	0.00014
1000	72.14	29.86	233.4	0.06	−181.611	0.00017
1000	81.97	26.28	103.5	0.06	−181.715	0.00016
1000	92.65	23.25	29.5	0.07	−181.756	0.00018
1500	61.01	35.31	533.9	0.08	−181.329	0.00039
1500	63.14	34.12	458.0	0.06	−181.400	0.00022
1500	67.54	31.89	332.8	0.07	−181.514	0.00021
1500	72.14	29.86	236.6	0.09	−181.600	0.00033
1500	81.97	26.28	106.4	0.09	−181.705	0.00027
1500	92.65	23.25	32.6	0.13	−181.746	0.00034
2000	61.01	35.31	536.9	0.10	−181.318	0.00037
2000	63.14	34.12	461.0	0.08	−181.389	0.00027
2000	67.54	31.89	335.6	0.08	−181.504	0.00027
2000	72.14	29.86	239.2	0.11	−181.591	0.00034
2000	81.97	26.28	109.4	0.17	−181.694	0.00054
2000	92.65	23.25	35.6	0.22	−181.735	0.00076
2500	61.01	35.31	539.5	0.14	−181.308	0.00038
2500	63.14	34.12	463.7	0.14	−181.379	0.00051
2500	67.54	31.89	338.6	0.10	−181.493	0.00032
2500	72.14	29.86	242.3	0.17	−181.579	0.00058
2500	81.97	26.28	112.5	0.15	−181.683	0.00046
2500	92.65	23.25	38.7	0.19	−181.725	0.00053
3000	61.01	35.31	542.5	0.11	−181.298	0.00037
3000	63.14	34.12	466.6	0.20	−181.368	0.00072
3000	67.54	31.89	341.1	0.16	−181.484	0.00057
3000	72.14	29.86	245.6	0.22	−181.568	0.00075
3000	81.97	26.28	115.1	0.23	−181.674	0.00068
3000	92.65	23.25	41.7	0.45	−181.714	0.00141

the effective Debye temperature Θ_D using

$$\langle u^2 \rangle = \frac{3h^2}{4\pi^2 M k_B \Theta_D}\left(\frac{D_1(\Theta_D/T)}{\Theta_D/T} + \frac{1}{4}\right), \qquad (2)$$

where $\vec{u}, M, h$ are the displacement vector, the ion mass, the Planck constant, and D_1 is the first-order Debye function. The quantum correction term $\frac{1}{4}$ shall be omitted in the classical treatment. Since the phonon density of states is not exactly Debye-like, this is the effective Debye temperature for the second moment of the vibrational density of states (VDOS), not exactly equal to the thermodynamic Debye temperature [29]. The residual is the deviation between the target function and the sample mean. From Fig. 2, we observe that the residuals are randomly distributed across the volume range. The absolute value of residuals for U and P are less than 0.002 Ry and 1.0 GPa (except for the data point at 3000 K). For the internal energy, a global minimum U_{min} is subtracted from the data set. On the scale of half Ry, the internal energy is well

represented. As for the pressure, we computed the pressure differences with respect to the $T = 300$ K reference and the fitted curves aligned with the data set. Only the $T = 3000$ K fit is slightly off. The resultant fitting coefficients in atomic units for both the Debye model and the classical model are tabulated (see Table II). The statistical summary from the *lm* function is included in Appendix A (see Fig. 12).

A. *P-V-T* EoS

The equilibrium atomic volume ($P = 0$ GPa) at 300 K is 14.559 Å^3, 2.9% larger than the experimental value 14.145 Å^3. The overestimation of the lattice constants is expected for the PBE exchange-correlation functional. Experimental P-V curves of the 300 K isotherm are readily compared with our theoretical predictions. Pressures measured by Akella *et al.* [5] are underestimated for compression (see Fig. 3), $\Delta V/V_0$ larger than 0.05 with $\Delta V = V_0 - V$. Overall the theoretical
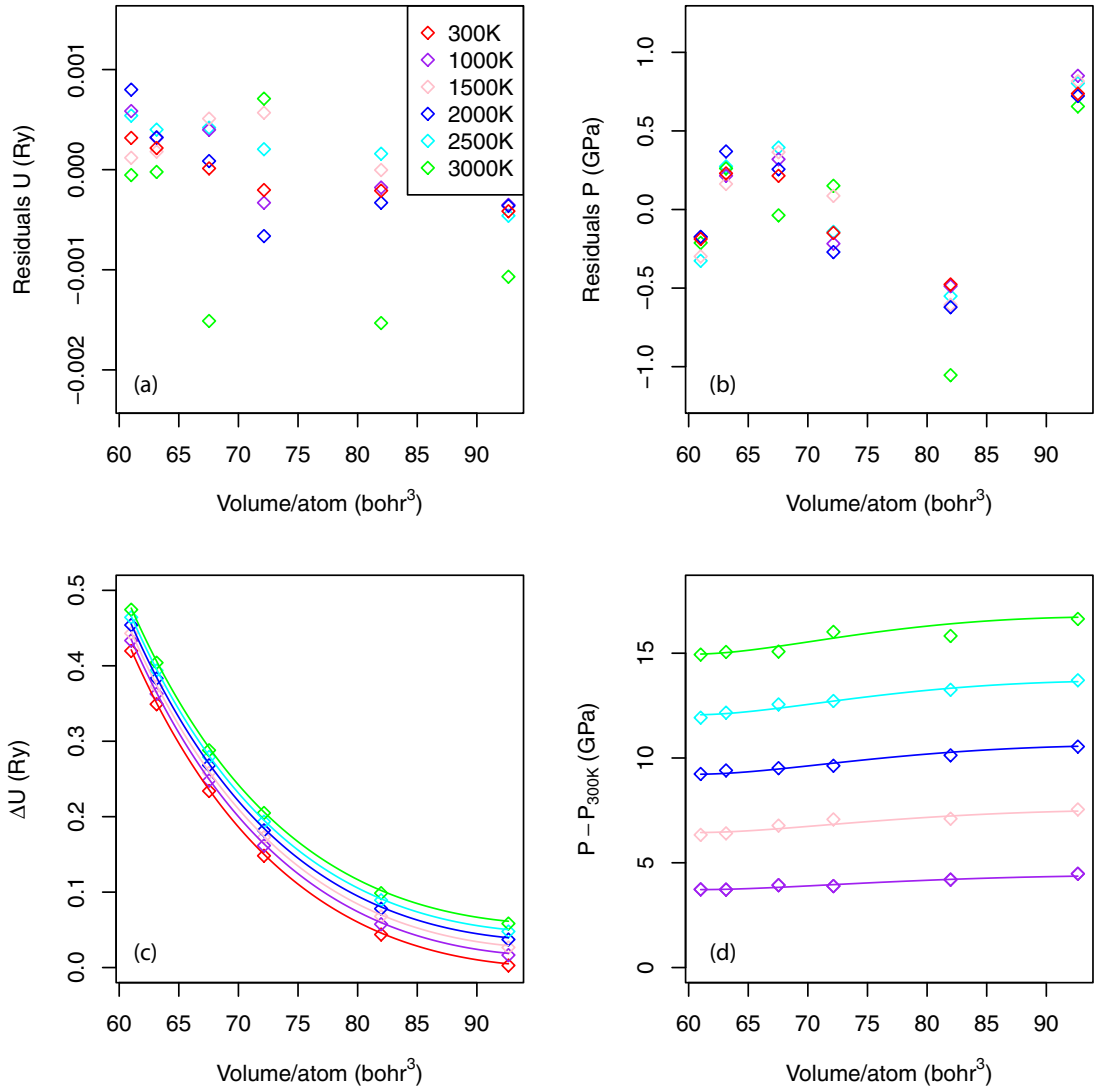
FIG. 2. The residuals of the fit to Eq. (1) for the EoS of fcc iridium are shown in (a) and (b). $\Delta U = U - U_{\min}$, where $U_{\min}$ is the minimum in the data set underlined in Table I. The fitted curves are compared against the data set in (c) and (d). ΔU and thermal pressure $P - P_{300K}$ from the fit align well against the data set.

300 K isotherm agrees well with the experiments within the uncertainty especially when the compression is smaller than 0.15 ($P < 70$ GPa) [6,10,30]. In contrast, the 3rd-order BM fit done by Monteseguro *et al.* [10] sits along our 1000 K isotherm for compression >0.15, and reflects the inadequacy of BM EoS at high compression. For comparison, we have

also included the FPMD and experimental study of Anzellini *et al.* [14]. Their *P-V-T* curves (both theory and experiments) below 80 GPa are obtained using the EoSFit7 package with ingredients such as the third-order BM EoS for the isothermal part. Their FPMD used the local density approximations and smaller energy cutoff (300 eV). The isotherm of 0 K com-

TABLE II. Coefficient matrix A in atomic units for the choice of F_0, the Debye model, and the classical model. The root mean squared errors (RMS) in the fitting for the pressure P (in GPa) and the internal energy U (in mRy) are listed.

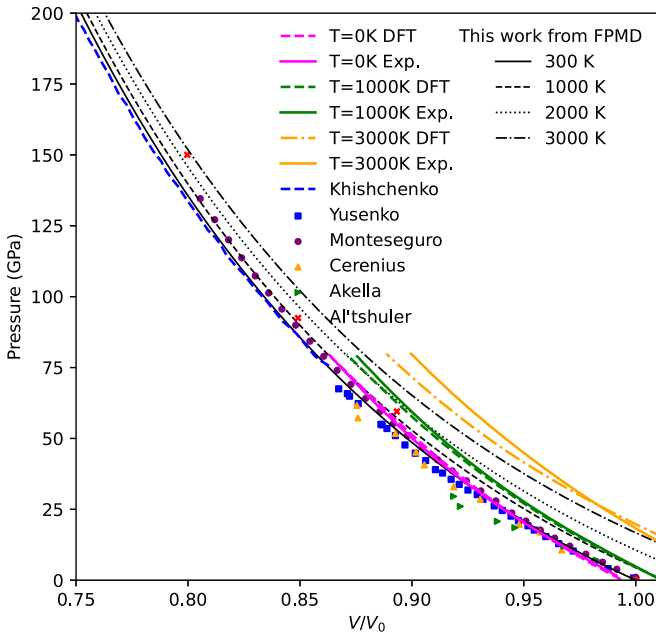|	A_{ij}			P RMS (GPa)	U RMS (mRy)
Debye model	1.904	-62.84	88.81	8175	0.5380	0.706
	0	0.008698	-0.1175	0.5574		
	6.681×10^{-09}	-3.752×10^{-07}	6.321×10^{-06}	-3.439×10^{-05}		
Classical model	1.902	-62.83	88.68	8176	0.5378	0.661
	0	0.008676	-0.1171	0.5549		
	6.567×10^{-09}	-3.667×10^{-07}	6.166×10^{-06}	-3.347×10^{-05}		

FIG. 3. Theoretical and experimental EoS's of fcc iridium are compared. The DAC experimental data for Yusenko [30], Monteseguro [10], Cerenius [6], and Akella [5] were compared at 300 K, where the BM EoS's were available. Experimental and theoretical data from Anzellini [14] are included (pink, green, and yellow lines). The shock wave data (red cross) of Al'tshuler were taken from Ref. [10]. Room temperature isotherm of Khishchenko shock experiments [34] agrees very well against our FPMD results.

pared well against our 300 K curve at low compression but not at high compression (compression >0.1), and similarly for the isotherms of 1000 K and 3000 K. The shock wave experiment by Al'tshuler *et al.* [31–33] exhibits quite distinct behavior in the *P-V* curve. Around compression of 0.1, the temperature is pinned slightly above the isotherm of 1000 K and at compression of 0.22 the temperature is close to the 3000 K isotherm. The high compression pressure ($\approx$600 GPa) of Al'tshuler *et al.* was mistakenly reported in Ref. [10]. The recent shock wave experimental work by Khishchenko [34] is also compared. We observe that the room temperature isotherm of recent work by Khishchenko aligns almost
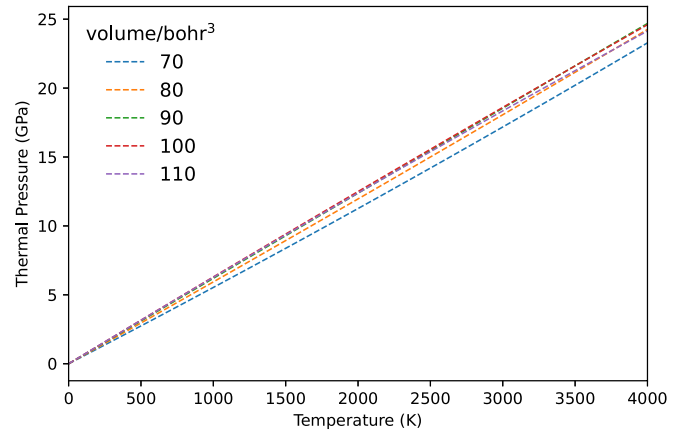

FIG. 4. The thermal pressure of fcc iridium is roughly linear in T.

perfectly with our EoS data. The data by Monteseguro *et al.* run along our 1000 K isotherm for compression over 0.1. It is well known that dynamic compression experiments lead to a temperature rise. Contrary to the claim that the temperature effect is negligible by Monteseguro *et al.* [10], we believe that the temperature increase (not measured) along the shock compression *P-V* curve is significant from our predicted EoS. Thermal pressure measures the pressure change upon temperature increase at constant volume, $P_{th}(V, T) = P(V, T) - P(V, T_0)$. The thermal pressure is quite linear in T given that αK_T (α and K_T are the thermal expansivity and the bulk modulus) is constant in the classical regime (above the Debye temperature), expressed as

$$P_{th}(V, T) = \int_{T_0}^{T} dT \left(\frac{\partial P}{\partial T}\right)_V = \int_{T_0}^{T} dT \, \alpha K_T. \qquad (3)$$

An oversimplified linear equation (see Fig. 4) could be given to the thermal pressure $P_{th}(T) = \lambda T$, with $\lambda = 0.0056$ GPa/K for the equilibrium volume. One could also see that the volume dependence is weak from the bottom right panel of Fig. 2.

The equilibrium bulk modulus B_0 (or inverse compressibility at room temperature and zero pressure) is an important parameter in the EoS formula, such as the Vinet EoS [35,36]. The fitted bulk modulus is compared against earlier studies

TABLE III. Experimental equilibrium volume V_0 (Å^3 per atom), bulk modulus B_0 (GPa), and B_0' at room temperature are compared against reported theoretical results. Data and method are briefly summarized, and the original references are given.

| Method description	V_0 (Å^3/at)	B_0 (GPa)	B_0'	References
Exp. data fitted to 3rd-order BM EoS	14.120	339	5.3	Monteseguro *et al.* [10]
Exp. data fitted to 3rd-order BM EoS	14.145	383	3.1	Cynn *et al.* [7]
Exp. data fitted to				Cerenius and Dubrovinsky [6]
2nd-order BM EoS, with $B_0' = 4$	14.173 (exp. value)	354	4.0	
3rd-order BM EoS, without constraint	14.173 (exp. value)	306	6.8	
DFT data fitted to BM EoS				Park *et al.* [37], Tables 1 and 2
PAW LDA	13.925	399		
PAW GGA	14.524	344		
FPMD data fitted to 3rd-order BM EoS	14.150	366	5.0	Burakovsky *et al.* [9]
FPMD data fitted to our EoS	14.559	361	5.3	This work
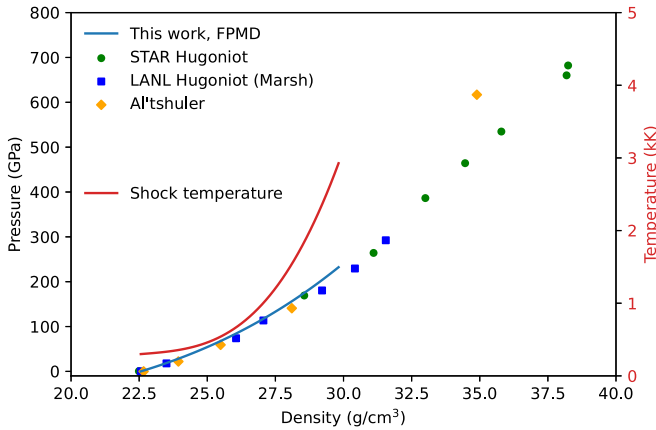
FIG. 5. The principle Hugoniot curve from our theoretical EoS (solid black) of fcc Ir is compared against the shockwave experimental data (symbols). Round green is for the STAR Hugoniot [41], square blue for the LANL Hugoniot [42], and diamond orange for Al'tshuler [31,32], respectively. Computed temperature from Eq. (4) is shown in red. The dashed extension is beyond the simulation domain.

(see Table III). We note that Cerenius and Dubrovinsky [6] obtained similar bulk modulus, 354 GPa versus 306 GPa, by fitting the second-order BM EoS with constraint $B_0' = 4$ or third-order BM EoS without constraint, both using experimental equilibrium volume. Park *et al.* obtained the bulk modulus of 399 GPa and 344 GPa for the LDA and GGA functional in DFT, respectively [37]. We note that B_0 from our fit is close to the accepted value of about 365 GPa and evidently smaller than Cynn's value 383 GPa [7]. The parameter B_0' from our model is 5.3.

B. Shock compression

High-pressure, high-temperature conditions are generated by laser heating [38] or resistive heating [39] in a DAC or by laser or gas gun [40] driven shock compression. Strong shocks obey the Rankine-Hugoniot,

$$U - U_0 + \frac{1}{2}(P + P_0)(V - V_0) = 0. \quad (4)$$

Since the analytical expression for U, P as a function of V, T is known, for each volume V, we solve Eq. (4) by searching its root T given the experimental value V_0, T_0.

We compared our predicted principle Hugoniot with available shock experimental data from several facilities [41,43] (Fig. 5). Our theoretical principle Hugoniot agrees well with that from earlier data of Al'tshuler and LANL March, as well as more recent data of STAR Hugoniot, for $P < 200$ GPa. Above 200 GPa, our predicted pressure is higher than that of LANL and STAR but lower than Al'tshuler's. Our theoretical Hugoniot below 3000 K (shock temperature) is fairly reliable which corresponds to pressure less than 200 GPa. The shock temperature, calculated as the solution to Eq. (4), is shown.

C. Equation of state parameters

Thermal EoS parameters such as thermal expansivity α, isothermal compressibility β_T, Grüneisen parameter γ, and the heat capacity C_V and C_P are obtained by differentiation
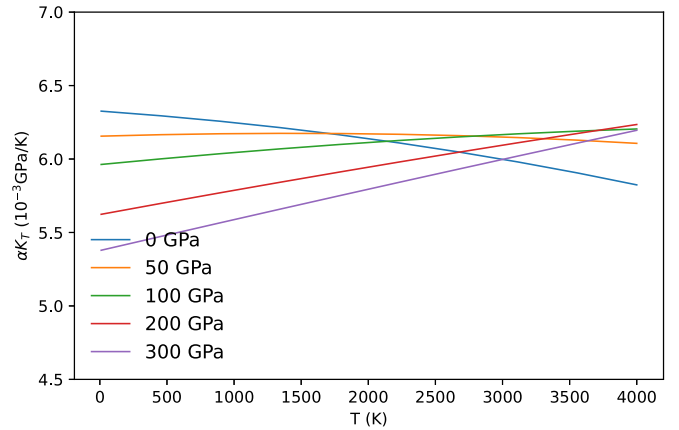

FIG. 6. Parameter αK_T as a function of temperature for various pressures.

and algebraic manipulation of Eq. (1). We now discuss some of these parameters. As expected from the thermal pressure, αK_T is weakly dependent on the volume and temperature (see Fig. 6). The Grüneisen parameter

$$\gamma = V\left(\frac{\partial P}{\partial U}\right)_V = V\frac{\alpha K_T}{C_V} \quad (5)$$

is another important parameter. It is used in the Mie-Grüneisen EoS, where γ is assumed independent of temperature. The span of γ as a function of temperature reduces when the pressure increases (see Fig. 7). For high compressions, it is indeed fairly temperature independent. The volumetric thermal expansivity $\alpha = -1/V(\partial V/\partial T)_P$ for isotropic materials is three times the linear thermal expansivity coefficient α_L, $\alpha = 3\alpha_L$. α in Fig. 8 is essentially temperature independent but rather volume sensitive. Our theoretical prediction is below the reported experimental value [44], but it is noted that around room temperature, our theory prediction gives the right thermal expansion coefficient. The expansivity has downsized by a factor of 4 when the pressure goes to 300 GPa. The heat capacity at high pressures is almost linear above 500 K; see Fig. 9. The higher the temperature, the slope of C_P is smaller. At 0 GPa, the predicted value 25.68 J K^{-1} mol^{-1}
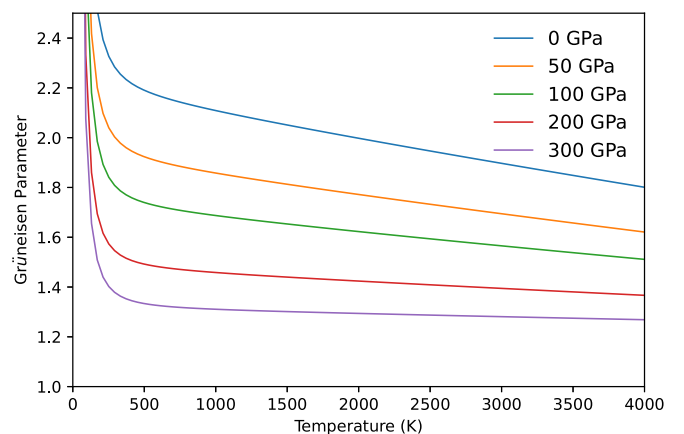

FIG. 7. Grüneisen parameter γ as a function of temperature for various pressures.
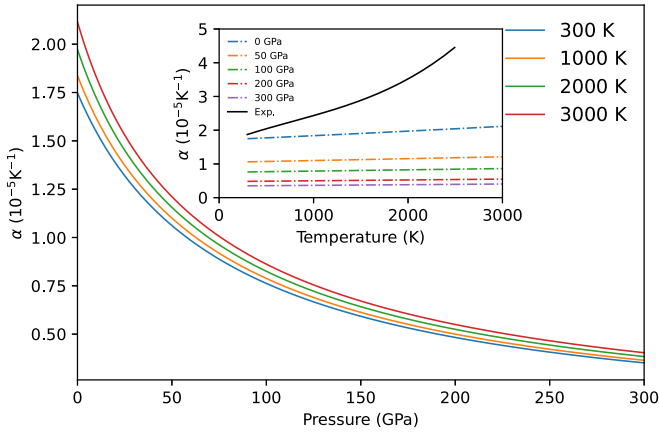
FIG. 8. The volumetric thermal expansivity α of fcc iridium as a function of pressure at various temperatures. Halvorson and Wimber measured the linear thermal expansion as $\alpha_t = a_0 + a_1 t + a_2 t^2 + a_3 t^3$ with $a_0 = 6.167 \times 10^{-6}$, $a_1 = 3.038 \times 10^{-9}$, $a_2 = -0.8448 \times 10^{-12}$, $a_3 = 0.5852 \times 10^{-15}$, for t expressed in °C [44] at ambient pressure (see inset solid line), where one can show $\alpha = 3(L_0/L_t)\alpha_t$ for isotropic materials with reference length L_0.

is fairly accurate and only 2.3% larger than the experimental heat capacity 25.10 J K^{-1} mol^{-1} [45], given that we used the formula $C_P = C_V(1 + T\alpha\gamma)$ (see Appendix A) with errors in C_V, α, and γ.

The RMSD is a critical quantity for the analysis of the phonon vibrations. Moseley *et al.* [46] presented temperature-
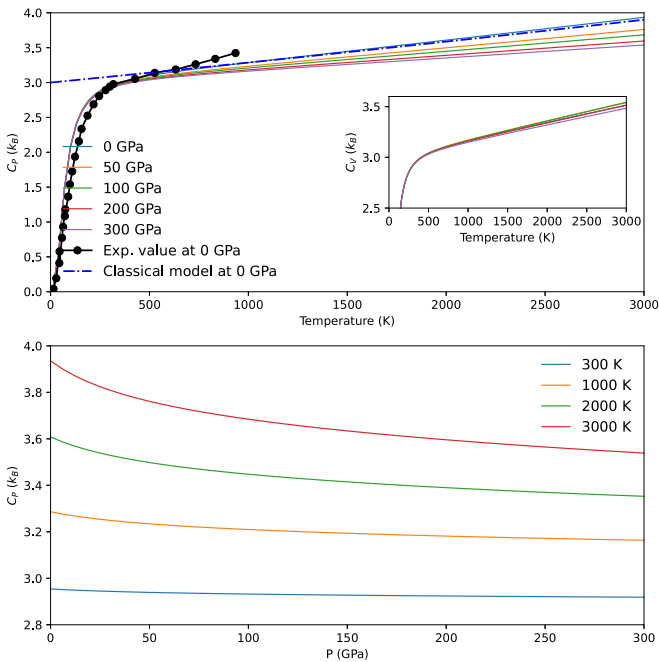

FIG. 9. Constant pressure heat capacity C_P as a function of temperature (top panel) and pressure (bottom panel). Experimental value at ambient condition is 25.10 J K^{-1} mol^{-1} [45]. The classical model (blue dash-dotted) for 0 GPa starts to deviate for T below 500 K, and approaches the classical limit as $T \to 0$ K. Inset shows the constant volume heat capacity C_V. Heat capacity largely reduces when pressure goes up.
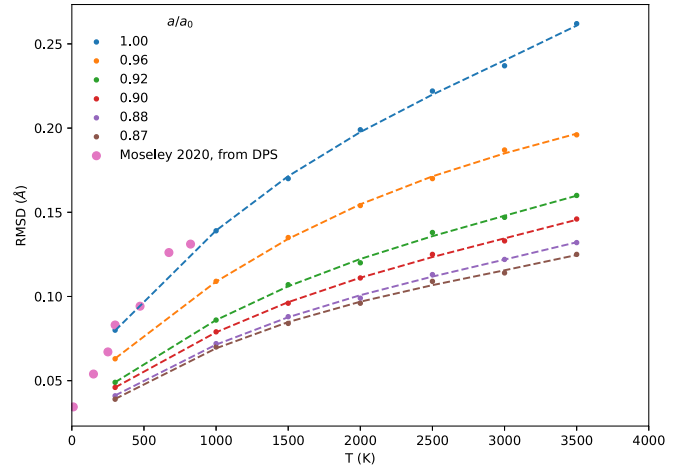

FIG. 10. RMSD as a function of temperature. Experimental data were obtained by Moseley *et al.* [46] for constant pressure.

dependent inelastic neutron scattering (INS) experiments as well as quasiharmonic density functional theory calculations to study the thermodynamic properties of Ir. Our FPMD RMSD at 300 K (see Fig. 10) agrees particularly well with their experimental findings. Their reported $\langle u^2 \rangle$ at higher temperatures ($T = 673$ K and 823 K; see Table I of Ref. [46]), however, are higher than our FPMD predictions. This is reasonable since our *NVT* ensembles at these temperatures lead to higher pressure and confined vibrations. It is worth noting that their phonon density of states (PDOS) integrates to 1, and is not fitted well at higher energies. Further investigation of PDOS with a FPMD simulation to compare against the experiments may give insight to the anharmonic effects. Debye temperatures of isochores using Eq. (2) exhibit weak temperature dependence (see Fig. 11).
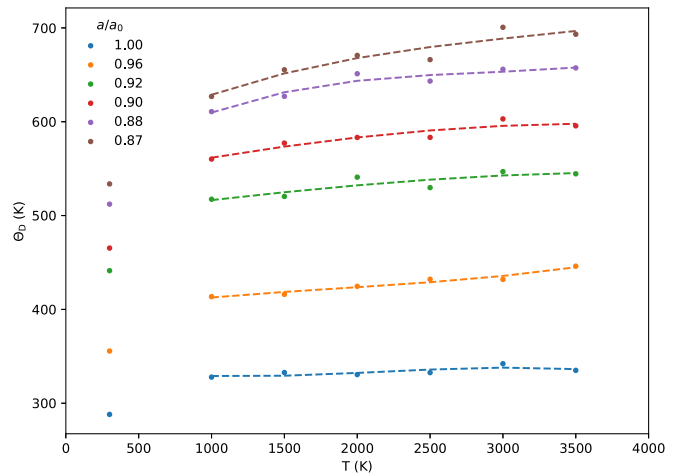

FIG. 11. Debye temperature Θ_D as a function of temperature. Zero-point motion is not included to obtain the Debye temperature. In the high-temperature, classical region, our RMSDs are classical from classical FPMD (Fig. 10), but when an effective classical Debye temperature is derived to model the RMSD, there is a large change with decreasing temperature to quantum regime in the Debye model. A 4th-order polynomial fit is done only for higher temperature due to the classical treatment to the ions.

IV. CONCLUSIONS

We have performed a series of FPMD simulations for the fcc Ir at conditions up to 3000 K and 540 GPa. By using a simplified model for the free energy as a function of temperature and volume and the statistical average quantities internal energy and pressure (U, P), the thermal EoS is obtained by globally fitting to the model. We have compared previous experimental EoS's and provided the thermal EoS up to 3000 K and 540 GPa. The *P-V-T* curve reasonably agrees with the fitted BM EoS at low compression but differs at high compression. Our first-principles EoS accords with the most recent shock wave experiment work by Khishchenko. We find that αK_T and the thermal pressure are quite constant from their dependence on temperature and which turns out to be true for a wide range of materials. We have shown some representative derived thermal parameters against available experiments and found agreements and discrepancies. Further work might resolve these discrepancies.

APPENDIX A: THERMODYNAMIC RELATIONS

Once the Helmholtz free energy $F = F(V, T)$ is known as a function of volume (V) and temperature (T), the following thermodynamical quantities can be obtained from it [47]:

$$P = -\left(\frac{\partial F}{\partial V}\right)_T, \tag{A1}$$

$$S = -\left(\frac{\partial F}{\partial T}\right)_V, \tag{A2}$$

$$K_T = \beta_T^{-1} = -V\left(\frac{\partial P}{\partial V}\right)_T = V\left(\frac{\partial^2 F}{\partial V^2}\right)_T, \tag{A3}$$

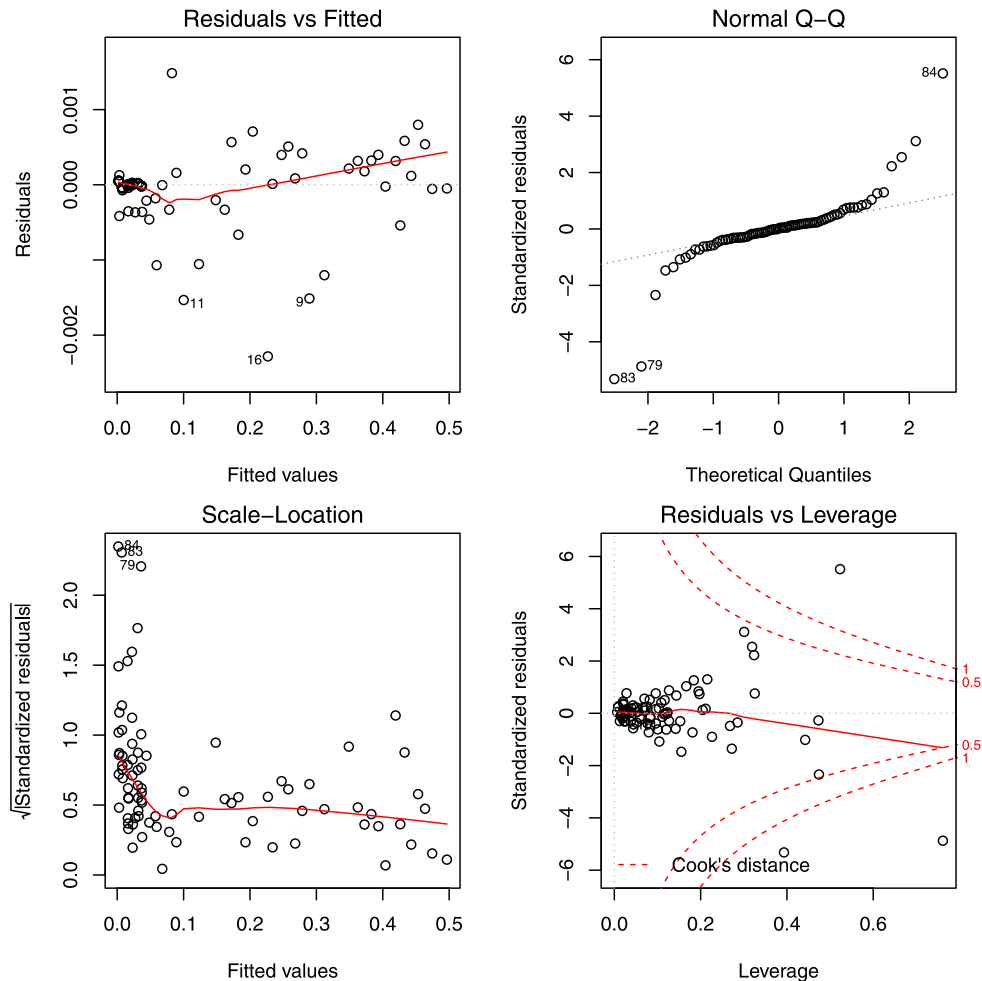

FIG. 12. The fit summary plot from the *lm* function in R.

$$C_V = T\left(\frac{\partial S}{\partial T}\right)_V = -T\left(\frac{\partial^2 F}{\partial T^2}\right)_V, \tag{A4}$$

$$\alpha K_T = -\left(\frac{\partial^2 F}{\partial T \partial V}\right), \tag{A5}$$

$$\gamma = V\left(\frac{\partial P}{\partial U}\right)_V = V\frac{\alpha K_T}{C_V}, \tag{A6}$$

$$\frac{C_P}{C_V} = \frac{K_S}{K_T} = 1 + T\alpha\gamma, \tag{A7}$$

$$U = F + TS, \tag{A8}$$

where pressure, entropy, isothermal compressibility (its inverse is the bulk modulus K_T), constant volume molar heat capacity, volumetric expansion coefficient, Grüneisen parameter, and internal energy are denoted by $P, S, \beta_T, C_V, \alpha, \gamma, U$. C_P is the constant pressure molar heat capacity. The parameter B'_0 (or $K'_0 = \frac{\partial K}{\partial P}|_{P=0}$) can thus be computed using the above relations:

$$K' = \frac{\partial K}{\partial P}$$

$$= \left(\frac{\partial K}{\partial T}\right)_V \left(\frac{\partial T}{\partial P}\right)_V + \left(\frac{\partial K}{\partial V}\right)_T \left(\frac{\partial V}{\partial P}\right)_T$$

$$= \left(\frac{\partial K}{\partial T}\right)_V \frac{1}{\left(\frac{\partial P}{\partial T}\right)_V} + \left(\frac{\partial K}{\partial V}\right)_T \frac{1}{\left(\frac{\partial P}{\partial V}\right)_T}$$

$$= \left(\frac{\partial K}{\partial T}\right)_V \frac{1}{\left(\frac{\partial P}{\partial T}\right)_V} - \left(\frac{\partial K}{\partial V}\right)_T \frac{V}{K_T}. \tag{A9}$$

APPENDIX B: DEBYE MODEL

The Helmholtz free energy F of a vibrating lattice at volume V and temperature T can be approximated as

$$F(V, T) = E(V) + F_{\text{vib}}(V, T) + F_{el}(V, T), \tag{B1}$$

where F_{vib} is the vibrating energy of the lattice and F_{el} is the thermal electronic free energy which is typically negligible. Moruzzi *et al.* [28] proposed an empirical Debye model with

$$F_{\text{vib}} = k_B T[-D_3(x) + 3\ln(1 - e^{-x})] + \frac{9}{8}k_B \Theta_D, \tag{B2}$$

with Debye temperature Θ_D and dimensionless parameter $x = \frac{\Theta_D}{T}$. The last term is the zero-point energy. $D_3(x)$ is the third-order Debye function. The nth-order Debye function is defined as

$$D_n(x) = \int_0^x \frac{t^n}{e^t - 1}dt, x \geqslant 0, \tag{B3}$$

where n, a non-negative integer, is the order of the Debye function. The vibrational entropy is

$$S_{\text{vib}} = 4k_B D(x) - 3k_B \ln(1 - e^{-x}). \tag{B4}$$

Neglecting the zero-point motion, the vibrational internal energy U_{vib} thus can be obtained:

$$U_{\text{vib}} = F_{\text{vib}} + TS_{\text{vib}} = 3k_B TD(x). \tag{B5}$$

[1] J. W. Arblaster, Platinum Metals Review **54**, 93 (2010).

[2] P. W. Bridgman, Proc. Am. Acad. Arts Sci. **71**, 387 (1937).

[3] P. W. Bridgman, Proc. Am. Acad. Arts Sci. **81**, 165 (1952).

[4] B. Schock and Q. Johnson, Fiz. Metal. Metalloved. **31**, 1101 (1971).

[5] J. Akella, J. Phys. Chem. Solids **43**, 941 (1982).

[6] Y. Cerenius and L. Dubrovinsky, J. Alloys Compd. **306**, 26 (2000).

[7] H. Cynn, J. E. Klepeis, C.-S. Yoo, and D. A. Young, Phys. Rev. Lett. **88**, 135701 (2002).

[8] S. Baroni, S. de Gironcoli, A. Dal Corso, and P. Giannozzi, Rev. Mod. Phys. **73**, 515 (2001).

[9] L. Burakovsky, N. Burakovsky, M. J. Cawkwell, D. L. Preston, D. Errandonea, and S. I. Simak, Phys. Rev. B **94**, 094112 (2016).

[10] V. Monteseguro, J. Sans, V. Cuartero, F. Cova, I. A. Abrikosov, W. Olovsson, C. Popescu, S. Pascarelli, G. Garbarino, H. J. M. Jönsson *et al.*, Sci. Rep. **9**, 8940 (2019).

[11] H. Fang, B. Liu, M. Gu, X. Liu, S. Huang, C. Ni, Z. Li, and R. Wang, Phys. B: Condens. Matter **405**, 732 (2010).

[12] G. Kaptay, J. Mater. Sci. **50**, 678 (2015).

[13] F. Birch, Phys. Rev. **71**, 809 (1947).

[14] S. Anzellini, L. Burakovsky, R. Turnbull, E. Bandiello, and D. Errandonea, Crystals **11**, 452 (2021).

[15] W. Kohn and L. J. Sham, Phys. Rev. **140**, A1133 (1965).

[16] N. D. Mermin, Phys. Rev. **137**, A1441 (1965).

[17] V. V. Karasiev, T. Sjostrom, J. Dufty, and S. B. Trickey, Phys. Rev. Lett. **112**, 076403 (2014).

[18] V. V. Karasiev, L. Calderín, and S. B. Trickey, Phys. Rev. E **93**, 063207 (2016).

[19] V. V. Karasiev, J. W. Dufty, and S. B. Trickey, Phys. Rev. Lett. **120**, 076401 (2018).

[20] P. Giannozzi, S. Baroni, N. Bonini, M. Calandra, R. Car, C. Cavazzoni, D. Ceresoli, G. L. Chiarotti, M. Cococcioni, I. Dabo, A. D. Corso, S. de Gironcoli, S. Fabris, G. Fratesi, R. Gebauer, U. Gerstmann, C. Gougoussis, A. Kokalj, M. Lazzeri, L. Martin-Samos, N. Marzari, F. Mauri, R. Mazzarello, S. Paolini, A. Pasquarello, L. Paulatto, C. Sbraccia, S. Scandolo, G. Sclauzero, A. P. Seitsonen, A. Smogunov, P. Umari, and R. M. Wentzcovitch, J. Phys.: Condens. Matter **21**, 395502 (2009).

[21] K. F. Garrity, J. W. Bennett, K. M. Rabe, and D. Vanderbilt, Comput. Mater. Sci. **81**, 446 (2014).

[22] J. P. Perdew, K. Burke, and M. Ernzerhof, Phys. Rev. Lett. **77**, 3865 (1996).

[23] J. P. Perdew, K. Burke, and M. Ernzerhof, Phys. Rev. Lett. **78**, 1396(E) (1997).

[24] See http://elk.sourceforge.net.

[25] G. Bussi, D. Donadio, and M. Parrinello, J. Chem. Phys. **126**, 014101 (2007).

[26] R. E. Cohen and O. Gülseren, Phys. Rev. B **63**, 224101 (2001).

[27] N. De Koker and L. Stixrude, Geophys. J. Int. **178**, 162 (2009).

[28] V. L. Moruzzi, J. F. Janak, and K. Schwarz, Phys. Rev. B **37**, 790 (1988).

[29] D. C. Wallace, Phys. Rev. **139**, A877 (1965).

[30] K. V. Yusenko, S. Khandarkhaeva, T. Fedotenko, A. Pakhomova, S. A. Gromilov, L. Dubrovinsky, and N. Dubrovinskaia, J. Alloys Compd. **788**, 212 (2019).

[31] L. V. Al'tshuler and A. A. Bakanova, Sov. Phys. Usp. **11**, 678 (1969).

[32] L. Al'Tshuler, A. Bakanova, I. Dudoladov, E. Dynin, R. Trunin, and B. Chekin, J. Appl. Mech. Tech. Phys. **22**, 145 (1981).

[33] V. V. Nemoshkalenko, V. Yu. Mil'man, A. V. Zhalko-Titarenko, V. N. Antonov, and Yu. L. Shitikov, Sov. JETP Lett. **47**, 295 (1988).

[34] K. V. Khishchenko, J. Phys.: Conf. Ser. **2154**, 012009 (2022).

[35] P. Vinet, J. Ferrante, J. R. Smith, and J. H. Rose, J. Phys. C **19**, L467 (1986).

[36] P. Vinet, J. R. Smith, J. Ferrante, and J. H. Rose, Phys. Rev. B **35**, 1945 (1987).

[37] J. Park, B. D. Yu, and S. Hong, Curr. Appl. Phys. **15**, 885 (2015).

[38] Y. Meng, G. Shen, and H. K. Mao, J. Phys.: Condens. Matter **18**, S1097 (2006).

[39] R. Boehler, Nature (London) **363**, 534 (1993).

[40] A. C. Mitchell and W. J. Nellis, Rev. Sci. Instrum. **52**, 347 (1981).

[41] C. Seagle, W. Reinhart, S. Alexander, J. Brown, and J.-P. Davis, Shock compression of iridium, in 21st Biennial Conference of the APS Topical Group on Shock Compression of Condensed Matter, 2019, https://www.osti.gov/servlets/purl/1640840.

[42] S. P. Marsh, *LASL Shock Hugoniot Data* (University of California Press, 1980).

[43] V. Fortov, L. Altshuler, R. Trunin, and A. Funtikov, *High-Pressure Shock Compression of Solids VII: Shock Waves and Extreme States of Matter*, Shock Wave and High Pressure Phenomena (Springer, New York, 2013).

[44] J. J. Halvorson and R. T. Wimber, J. Appl. Phys. **43**, 2519 (1972).

[45] D. R. Lide, *CRC Handbook of Chemistry and Physics*, Vol. 85 (CRC Press, 2004).

[46] D. H. Moseley, S. J. Thébaud, L. R. Lindsay, Y. Cheng, D. L. Abernathy, M. E. Manley, and R. P. Hermann, Phys. Rev. Mater. **4**, 113608 (2020).

[47] H. B. Callen, *Thermodynamics and an Introduction to Thermostatistics* (American Association of Physics Teachers, 1998).